Proceedings of the IASTED International Conference
ROBOTICS AND APPLICATIONS
October 31 - November 2, 2005, Cambridge, USA

FORCE CONTROL LAW DESIGN FOR A FIVE DEGREE-OF-FREEDOM HAPTIC MECHANISM

Kostas Vlachos, and Evangelos Papadopoulos
Department of Mechanical Engineering, National Technical University of Athens
15780 Athens, Greece
{kostaswl, egpapado}@central.ntua.gr

ABSTRACT
In this paper the effect of a force control law in the transparency of a five degree-of-freedom (dof) haptic mechanism is investigated. The mechanism, which is a part of a training medical simulator for urological operations, consists of a two-dof, five bar linkage and a three-dof spherical joint. The force control algorithm is described and discussed. The open and closed loop schemes are compared. It is shown that the use of the control law aims at the maximization of the haptic device transparency increasing the realism of the simulation. A stability analysis of a one-dof haptic device is performed determining the force control law margin, i.e. a quantitative indication of the haptic mechanism ability to simulate a wide range of virtual environments, maintaining at the same time its stability. Simulation results of the force control law application on the five-dof mechanism are presented and discussed. The closed loop system shows substantially improved response with respect the open loop system.

KEY WORDS
Haptic, force control, force feedback, simulator.

1. Introduction

Virtual Reality is now an accepted tool in areas ranging from mechanical design to entertainment and medical training. During the past several years, research on the maximization of the virtual environment realism has introduced the haptic devices, [1]. The quality of a haptic device is often measured by its transparency characteristics. Transparency is associated with the absence of haptic device-induced parasitic torques/forces during its motion, e.g. mass/inertia, gravity forces and friction. Transparency is even more important for haptic devices used in simulators, where reality must be simulated reliably. There are two ways to maximize the haptic mechanism transparency, a) optimized design resulting in haptic mechanisms with minimum device-induced parasitic torques/forces, and b) design of a control law. All control laws designed for a haptic mechanism have the following goals, a) to secure the stability of the haptic device, and b) to maximize its transparency.

One can distinguish two trends in the control law design for haptic mechanisms. The first is characterized by the fact that the control law is designed taking into account the specific virtual environment. Minsky *et al.* in [2] used impedance control for a haptic joystick and presented a relationship between sampling rate, virtual environment stiffness, damping and the system stability. A PID force control law is presented in [3] by Birglen *et al.* to control the 3-dof haptic device SHaDe. Carignan and Cleary investigated several control methodologies in [4]. Furthermore, an adaptive control schema using active observers is proposed by Cortesão *et al.* in [5].

The second trend in the control law design for haptic devices is characterized by the separation of the control design from the virtual environment. According to this, Colgate *et al.* presented in [6] the use of a virtual coupling between the haptic mechanism and the virtual environment and the necessary coupling conditions for system stability. A virtual coupling consisting of a virtual spring-dumper using a "god-object" approach was introduced by Zilles and Salisbury in [7]. Adams and Hannaford used in [8] and [9] the two-port framework, a method rooted in linear circuit theory, to solve the problem of stable haptic simulation. They consider the haptic interface as the mechanical analog to an electrical two-port, under variable loading conditions both at user and virtual environment sides. Gil *et al.* presents the application of the Routh-Hurwitz criterion to study the stability of a 1-dof haptic device, [10]. Another approach, presented in [11] by Hannaford and Ryu, is the use of an energy-based method to guarantee the system stability using a "Passivity Observer" and a "Passivity Controller". These methods trying to guarantee system stability independently from the virtual environment give rather conservative results, and sometimes requires additional computational load. Furthermore Miller *et al.* investigates how virtual environment can be designed to guarantee the system stability, [12].

In this paper the effect of a force control law in the transparency of a five degree-of-freedom (dof) haptic

mechanism is investigated. The mechanism, which is a part of a training medical simulator for urological operations, consists of a two-dof, five bar linkage and a three-dof spherical joint. The force control algorithm is described and discussed. The open and closed loop schemes are compared. It is shown that the use of the control law aims at the maximization of the haptic device transparency increasing the realism of the simulation. A stability analysis of a one-dof haptic device is performed determining the force control law margin, e.g. a quantitative indication of the haptic mechanism ability to simulate a wide range of virtual environments, maintaining at the same time its stability. Simulation results of the force control law application on the five-dof mechanism are presented and discussed. The closed loop system shows substantially improved response with respect the open loop system.

2. Haptic Mechanism Description

As mentioned above, the haptic mechanism, which is our plant under control, is used in a training simulator for urological operations, developed by the authors, [13]. A urological operation can be divided in two phases, the insertion and the main operation, [13]. During insertion, the surgeon moves the tip of the endoscope along the urethra path from the insertion point A to the final point C at the bladder, via an intermediate point B, see Fig. 1. At point B, the endoscope orientation changes without translation, so as to align the entire urethra and continue the insertion without traumas. The corresponding endoscope poses are labeled by a, b, c, and d, in Fig. 1. During the main operation, the endoscope rotates in all directions but its tip translates minimally. These observations reveal that although the endoscope can have any orientation in a cone, its tip translations occur on the plane of symmetry of the patient x-y, see Fig. 1.

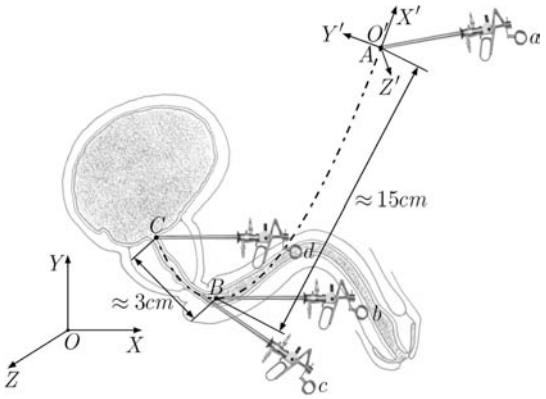

Fig. 1. Endoscope endpoint path and orientation during a urological operation.

These observations during our previous work showed that a haptic mechanism with two translational and three rotational dof is needed, [13]. The actual kinematical requirements that define the minimum workspace of the haptic interface were found by observations of typical urological operations. These resulted in a tool displacement requirement along the X and Y axes equal to 0.1 m, while rotation requirements around the X′ is ±180° and around the Z′ and Y′ is ±30°. The resulted haptic mechanism consists of a two dof, 5-bar linkage and a three dof spherical joint. Fig. 2 shows the first prototype of the haptic mechanism together with the other elements of the training urological simulator during a test session.

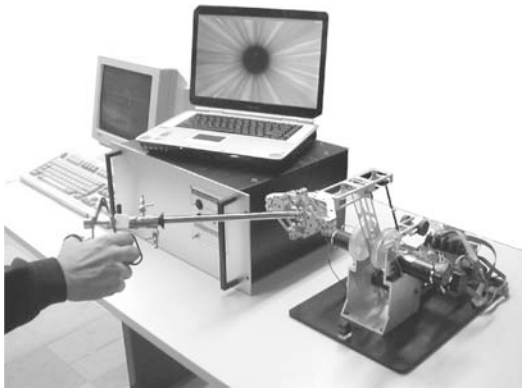

Fig. 2. Haptic mechanism, part of the training urological simulator during a test session.

The measured maximum endoscope forces are 4.5 N along the x and y axes. The maximum measured torques are 150 mNm about the endoscope fixed y' and x' axes and 10 mNm about the z' axis.

As mentioned above, the quality of a haptic device is often measured by its transparency characteristics. A great effort was given by the authors in [14] and [15] to design an optimum haptic mechanism, i.e. the best mechanical design under given kinematical, operational and constructional constraints. However, although optimization is required and must always be employed first, it cannot eliminate completely devise parasitic forces and torques and achieve perfect transparency. In principle, this can be done using a control strategy that compensates for the parasitic terms. However, in practice this is hard to achieve due to the difficulty of identifying all terms contributing to the parasitic terms and in addition requires larger than needed motors and inertias. A combination of the optimization and control approaches can further enhance the performance of a haptic device.

3. Open Loop Control

We consider first the open loop control law, where coreless DC motors actuate the device and apply torques aiming at giving the feeling that only the endoscope and the tissues are present. To compute the necessary motor currents, the equations of motion of the surgical tool during a real surgical operation, see Fig. 3, are written as

$$\mathbf{M}_t \dot{\mathbf{v}}_{cm} + \mathbf{V}_t + \mathbf{G}_t = \mathbf{F} + \mathbf{F}_r \qquad (1)$$

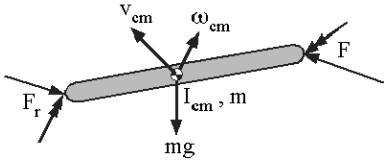

Fig. 3. Forces on surgical tool during a real surgical operation.

where $\mathbf{F}$ is the vector of the applied forces and torques by the operator to the tool, $\mathbf{M}_t$ is its mass matrix, $\mathbf{V}_t$ contains velocity terms, $\mathbf{G}_t$ contains gravity terms, and v_{cm} is the velocity of its center of mass. The vector $\mathbf{F}_r$ contains forces and torques, which are due to tissue deformation. Since no motion is allowed in the Z direction, in the virtual environment, $\mathbf{M}_t$ is a 5×5 matrix and the rest of the vectors have appropriate dimensions.

Furthermore, the equations of motion of the surgical tool attached at the haptic mechanism end effector during a simulated surgical operation, see Fig. 4, are written as

$$\mathbf{M}_t\dot{\mathbf{v}}_{cm} + \mathbf{V}_t + \mathbf{G}_t = \mathbf{F} + \mathbf{F}_T \qquad (2)$$

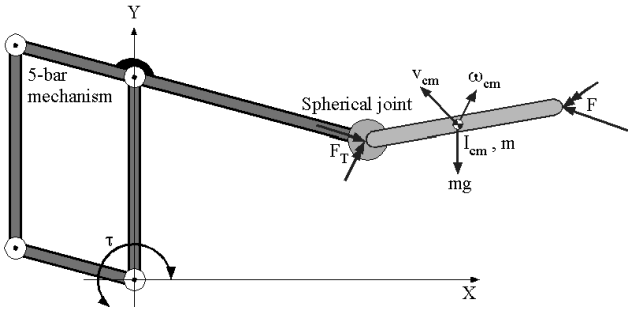

Fig. 4. Forces on surgical tool during a simulated surgical operation.

The vector $\mathbf{F}_T$ contains forces and torques, by the haptic mechanism to the surgical tool. In order to build a transparent haptic device the user must feel during the simulation the real forces and torques, which are due to tissue deformation. In other words our goal is to find the vector $\boldsymbol{\tau}$ of the actuators torques, so that vector $\mathbf{F}_T$ is equal vector $\mathbf{F}_r$. The equations of motion of the haptic mechanism during a simulated surgical operation, see Fig. 4, are written as

$$\mathbf{M}_m\dot{\mathbf{v}} + \mathbf{V}_m + \mathbf{G}_m = \mathbf{J}^{-T}\boldsymbol{\tau} - \mathbf{F}_T \qquad (3)$$

where $\mathbf{J}^{-T}\boldsymbol{\tau}$ is the vector of the applied torques by the actuators resolved as forces and torques at the end effector, $\mathbf{M}_m$ is the haptic mechanism mass matrix, $\mathbf{V}_m$ contains velocity terms, $\mathbf{G}_m$ contains gravity terms. Since no motion is allowed in the Z direction, in the virtual environment, $\mathbf{M}_m$ is a 5×5 matrix and the rest of the vectors have appropriate dimensions. Replacing $\mathbf{F}_T$ with $\mathbf{F}_r$, Eq. (3) became

$$\mathbf{M}_m\dot{\mathbf{v}} + \mathbf{V}_m + \mathbf{G}_m = \mathbf{J}^{-T}\boldsymbol{\tau} - \mathbf{F}_r \qquad (4)$$

From Eq. (4) we find that the vector $\boldsymbol{\tau}$ of the actuators torques, so that the user feels during the simulation the real forces and torques, which are due to tissue deformation is the following,

$$\boldsymbol{\tau} = \mathbf{J}^T(\mathbf{M}_m\dot{\mathbf{v}} + \mathbf{V}_m + \mathbf{G}_m + \mathbf{F}_r) \qquad (5)$$

In general, the forces and torques $\mathbf{F}_r$ are functions of the position and velocity of the tool and are computed based on a simplified model of tissue deformation as

$$\mathbf{F}_r = \mathbf{F}_r(\dot{\mathbf{q}}, \mathbf{q}) \qquad (6)$$

A detailed description of such a tissue model can be found in [16]. Finally, the control commands to the motor amplifiers are the following

$$\mathbf{u} = (\mathbf{K}_T\mathbf{K}_{amp})^{-1}\mathbf{J}^T(\mathbf{M}_m\dot{\mathbf{v}} + \mathbf{V}_m + \mathbf{G}_m + \mathbf{F}_r) \qquad (7)$$

where $\mathbf{K}_T$, and $\mathbf{K}_{amp}$ are diagonal matrices that contain motor torque constants and amplifier gains, respectively.

Next, the simulation results of the open loop control on the 5-dof haptic mechanism are described. It is obvious, see Eq. (6), that the tissue deformation model is function of the position and velocity of the tool. In order to test the open loop control, we record a typical endoscope tip motion during a testing session. The Cartesian space motion is shown in Fig. 5, and the resulting motor angle histories are displayed in Fig. 6.

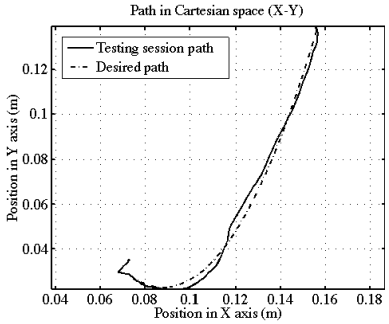

Fig. 5. Testing session endoscope tip motion and a typical desired path.

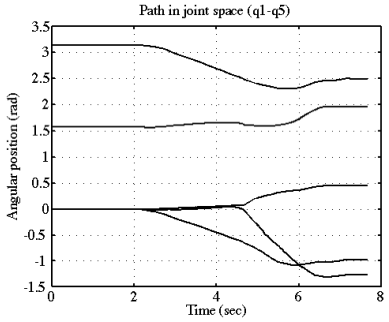

Fig. 6. Actuator space histories of the Testing session endoscope tip motion in Fig. 5.

The doted line in Fig. 5 shows the typical desired path that the user should follow according to Fig. 1. The error between the actual path and the desired one defines the value of the torques/forces that the user should feel according to a simple tissue deformation model modeled as a spring. The torques/forces are calculated according to the following relation,

$$\mathbf{F}_r = \mathbf{K}_r \mathbf{x}_e + \mathbf{B}_r \mathbf{v} \tag{8}$$

where $\mathbf{K}_r$, and $\mathbf{B}_r$ are diagonal matrices that contain spring constants and dumping coefficients, respectively. The vector $\mathbf{x}_e$ contains the position errors between the actual path and the desired one. Finally $\mathbf{v}$ is the Cartesian and angular velocities vector.

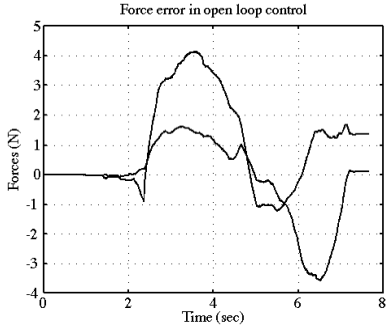

Fig. 7. Desired forces according to testing session path in Fig. 5.

Fig. 7 shows the desired forces according to testing session path in Fig. 5. Replacing Eq. (8) in Eq. (5) the vector $\boldsymbol{\tau}$ of the actuators torques, so that the user feels during the simulation the real forces and torques, which are due to tissue deformation is the following,

$$\boldsymbol{\tau} = \mathbf{J}^T(\mathbf{M}_m \dot{\mathbf{v}} + \mathbf{V}_m + \mathbf{G}_m + \mathbf{K}_r \mathbf{x}_e + \mathbf{B}_r \mathbf{v}) \tag{9}$$

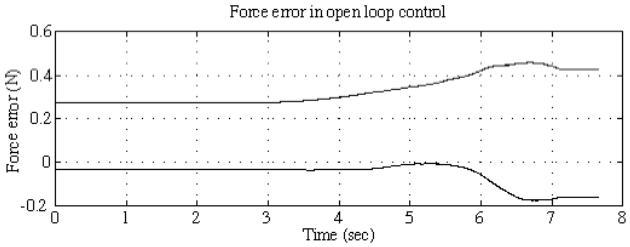

Fig. 8. Force errors in the open loop control.

Fig. 8 shows the open loop error at the forces that the user should feel during the testing session shown in Fig. 5 and according to Eq. (9). From Fig. 8 we can see that the signal has a permanent error of 0.2N to 0.4N. We already mentioned in the introduction that the measured maximum endoscope forces are 4.5 N along the x and y axes, which gives us a rather big error of about 5% to 10%.

It is shown that the haptic mechanism under open loop control cannot reliable simulate the virtual environment. This is expected because of various factors like errors in the haptic mechanism model or not modeled nonlinearities like friction. In order to overcome this problem we apply the following closed loop force control schema.

4. Closed Loop Control

The closed loop force control block diagram is presented in Fig. 8. The desired value that our plant, the "haptic mechanism" block, should output is the desired force, F_{des}, which is calculated in the "Virtual Environment" block according Eq. (8). The error between the desired force, F_{des}, and the output of the force sensor F_{sen}, is F_{err}, which is fed into the PI "Controller" block. The sensor output is subjected to noise. The haptic mechanism input is then calculated according to the following control law

$$\mathbf{F}_{in} = \mathbf{F}_{des} + (\mathbf{F}_{err}\mathbf{K}_p + \mathbf{K}_i \int \mathbf{F}_{err} dt) \tag{10}$$

Replacing the desired force F_{des}, with the virtual environment output according Eq. (8), The haptic mechanism input is the following

$$\mathbf{F}_{in} = \mathbf{K}_r \mathbf{x}_e + \mathbf{B}_r \mathbf{v} + (\mathbf{F}_{err}\mathbf{K}_p + \mathbf{K}_i \int \mathbf{F}_{err} dt) \tag{11}$$

Finally the vector $\boldsymbol{\tau}$ of the actuators torques is the following

$$\begin{aligned} \boldsymbol{\tau} = \mathbf{J}^T(\mathbf{M}_m \dot{\mathbf{v}} + \mathbf{V}_m + \mathbf{G}_m + \mathbf{K}_r \mathbf{x}_e + \mathbf{B}_r \mathbf{v} \\ + (\mathbf{F}_{err}\mathbf{K}_p + \mathbf{K}_i \int \mathbf{F}_{err} dt)) \end{aligned} \tag{12}$$

where $\mathbf{K}_p$, and $\mathbf{K}_i$ are vectors that contain the proportional and integral controller gains, respectively.

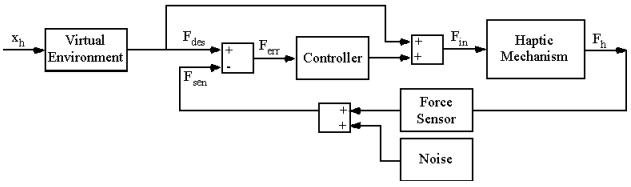

Fig. 9. Closed loop force control block diagram.

Fig. 9 shows the closed loop error at the forces that the user should feel during the testing session shown in Fig. 5 and according to Eq. (9). It is obvious that the error converges to zero, and the noise almost vanishes.

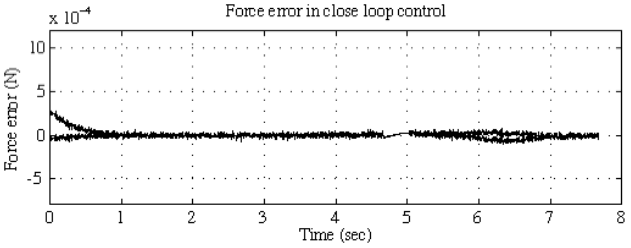

Fig. 10. Force errors in the closed loop control.

Next, some issues on stability are discussed. For simplicity, the analysis uses a 1-dof system shown in Fig. 10a.

5. Stability issues

The haptic mechanism has to simulate the virtual environment, which is modeled as a 1-dof spring-dumper system shown in Fig. 10b. The equation of motion of the 1-dof haptic device is written as

$$M\ddot{x} = F_{ext} - F_{in} - B\dot{x} \tag{13}$$

where M is the 1-dof haptic mechanism mass, $\dot{x}$ and $\ddot{x}$ its velocity and acceleration respectively, B the viscous friction coefficient, F_{ext} the external force by the user, and F_{in} the actuator force.

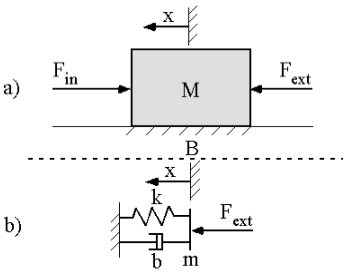

Fig. 11. a) 1-dof system, b) Virtual environment.

Assuming that the external force by the user, F_{ext}, is the same in both cases of Fig. 10, our goal is to determine the necessary actuator force F_{in}, see Fig. 10a, in order to feel the user the same force feedback as in Fig. 10b. The equation of motion of the virtual environment is written as

$$\begin{aligned} m\ddot{x} &= F_{ext} - b\dot{x} - kx \Rightarrow \\ \Rightarrow F_{ext} &= m\ddot{x} + b\dot{x} + kx \end{aligned} \tag{14}$$

where m is the 1-dof virtual object mass, $\dot{x}$ and $\ddot{x}$ the velocity and acceleration respectively of the virtual object mass, k the virtual spring constant, b the virtual viscous friction coefficient, and F_{ext} the external force by the user. Replacing F_{ext} from Eq. (14) to Eq. (13), the actuator force F_{in} is written as

$$\begin{aligned} M\ddot{x} &= m\ddot{x} + kx + b\dot{x} - F_{in} - B\dot{x} \Rightarrow \\ \Rightarrow F_{in} &= -M\ddot{x} + m\ddot{x} + kx + b\dot{x} - B\dot{x} \Rightarrow \\ \Rightarrow F_{in} &= (m-M)\ddot{x} + (b-B)\dot{x} + kx \end{aligned} \tag{15}$$

The transfer function between the system input, which is the actuator force F_{in}, and the system output, the translation x, is the following.

$$X(s) / F_{in}(s) = 1 / \{(m-M)s^2 + (b-B)s + k\} \tag{16}$$

Fig. 11 shows the closed loop force control block diagram of the 1-dof haptic mechanism. It is assumed that the force sensor is ideal and that the user hand position, x_h, velocity, v_h, and acceleration, a_h, are inputs to the system. According to this input, F_{des} the desired force is calculated using the equation

$$F_{des} = ma_h + kx_h + bv_h \tag{17}$$

and fed into the haptic mechanism together with the controller output. Input to the controller is the error between the desired force F_{des} and the sensor output F_{sen}.

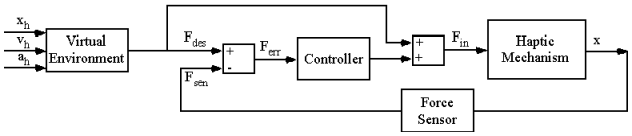

Fig. 12. Closed loop force control block diagram of the 1-dof haptic mechanism.

The transfer function of the closed loop is $Num / Denum$, where

$$\begin{aligned} Num &= -K_i k^2 - k(bK_i + k + K_p k)s - \\ &\quad k(b + bK_p + K_d k + K_i m)s^2 - \\ &\quad k(bK_d + m + K_p m)s^3 - K_d kms^4 \\ Denum &= K_i k + (bK_i - k + K_p k)s + \\ &\quad (B - b + bK_p + K_d k + K_i m)s^2 + \\ &\quad (bK_d + M - m + K_p m)s^3 + K_d ms^4 \end{aligned} \tag{18}$$

K_p, K_i, and K_d are the proportional, integral, and derivative controller gains, respectively, see Fig. 11. The root locus graph for the controller gain C, of the 1-dof haptic system is shown in Fig 12.

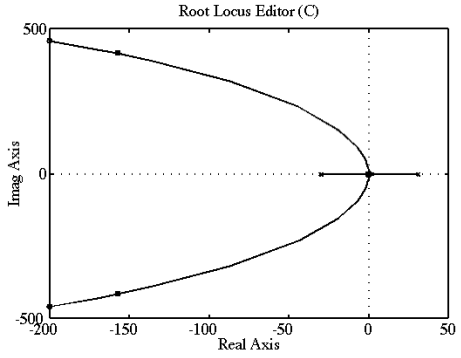

Fig. 13. Root locus of the 1-dof haptic mechanism of Fig. 10.

The system is stable for a virtual environment and controller gains as shown in Table 1.

Table 1
Closed loop parameters

Parameter	Value
Virtual spring constant, k	331 N/m
Virtual viscosity, b	0.4 Ns/m
Proportional gain, K_p	1000.0
Derivative gain, K_d	0.0
Integral gain, K_i	100.0

The virtual spring constant, and viscosity values are typical for our application, i.e. manipulating human soft tissues. It is important to notice that the system maintain

its stability even for large spring constant values like $k = 2483$. This would be useful if, for example, the haptic simulator has to simulate contact with a bone. Fig 13 presents the response in step input of the desired force.

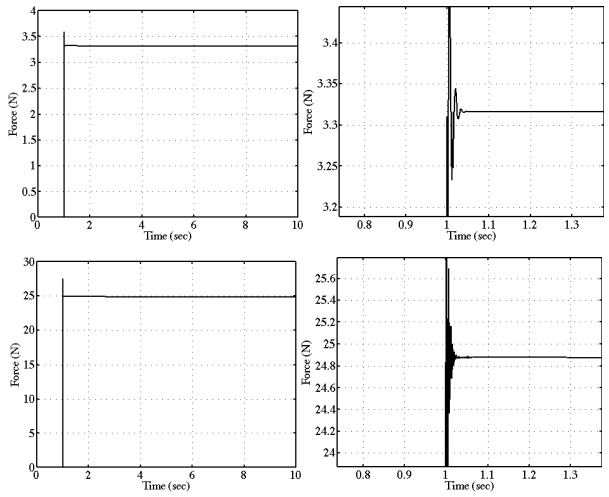

Fig. 14. Responses in step input.

6. Conclusion

In this paper the effect of a force control law in the transparency of a five degree-of-freedom (dof) haptic mechanism is investigated. The mechanism, which is a part of a training medical simulator for urological operations, consists of a two-dof, five bar linkage and a three-dof spherical joint. The force control algorithm is described and discussed. The open and closed loop schemes are compared. It is shown that the use of the control law aims at the maximization of the haptic device transparency increasing the realism of the simulation. A stability analysis of a one-dof haptic device is performed determining the force control law margin, e.g. a quantitative indication of the haptic mechanism ability to simulate a wide range of virtual environments, maintaining at the same time its stability. Simulation results of the force control law application on the five-dof mechanism are provided and discussed. The closed loop system shows substantially improved response with respect the open loop system.

Acknowledgements

This work is co-funded by the European Social Fund (75%) and National Resources (25%) – (EPEAEK II) – PYTHAGORAS.

References

[1] G. C. Burdea, *Force and touch feedback for virtual reality* (New York, NY: John Wiley & Sons, Inc., 1996).

[2] M. Minsky, M. Ouh-young, O. Steele, F. P. Brooks, Jr., & M. Behensky, Feeling and Seeing: Issues in Force Display, *Computer Graphics, 24* (2), 1990, 235-243.

[3] L. Birglen, C. Gosselin, N. Pouliot, B. Monsarrat, & T. Laliberté, SHaDe, A New 3-DOF Haptic Device, *IEEE Transactions on Robotics and Automation, 18* (2), 2002, 166-175.

[4] C. R. Carignan, & K. R. Cleary, Closed-Loop Force Control for Haptic Simulation of Virtual Environments, *Haptics-e, 1* (2), 2000.

[5] R. Cortesão, J. Park, & O. Khatib, Real-Time Adaptive Control for Haptic Manipulation with Active Observers, *Proc. IEEE/RSJ Int. Conference on Intelligent Robots and Systems*, Las Vegas, Nevada, 2003, 2938-2943.

[6] J. E. Colgate, M. C. Stanley, & J. M. Brown, Issues in the Haptic Display of Tool Use, *Proc. IEEE/RSJ Int. Conference on Intelligent Robots and Systems*, Pittsburgh, PA, 1995, 140-145.

[7] C. B. Zilles, & J. K. Salisbury, A Constraint-Based God-Object Method for Haptic Display, *Proc. IEEE/RSJ Int. Conference on Intelligent Robots and Systems*, Pittsburgh, PA, 1995, 146-151.

[8] R. J. Adams, & B. Hannaford, Stable Haptic Interaction with Virtual Environments, *IEEE Transactions on Robotics and Automation, 15* (3), 1999, 465-474.

[9] R. J. Adams, & B. Hannaford, Control Law Design for Haptic Interfaces to Virtual Reality, *IEEE Transactions on Control Systems Technology, 10* (1), 2002, 3-13.

[10] J. J. Gil, A. Avello, Á. Rubio, & J. Flórez, Stability Analysis of a 1 DOF Haptic Interface Using the Routh-Hurwitz Criterion, *IEEE Transactions on Control Systems Technology, 12* (4), 2004, 583-588.

[11] B. Hannaford, & J. Ryu, Time-Domain Passivity Control of Haptic Interfaces, *IEEE Transactions on Robotics and Automation, 18* (1), 2002, 1-10.

[12] B. E. Miller, J. E. Colgate, & R. A. Freeman, Guaranteed Stability of Haptic Systems with Nonlinear Virtual Environments, *IEEE Transactions on Robotics and Automation, 16* (6), 2000, 712-719.

[13] K. Vlachos, E. Papadopoulos, & D. N. Mitropoulos, Design and implementation of a haptic device for training in urological operations, *IEEE Transactions on Robotics and Automation, 19* (5), 2003, 801-809.

[14] K. Vlachos, E. Papadopoulos, & D. N. Mitropoulos, Mass/Inertia and Joint Friction Minimization for a Low-force Five-dof Haptic Device, *Proc. IEEE Int. Conference on Robotics and Automation*, New Orleans, Louisiana, 2004, 286-291.

[15] K. Vlachos, & E. Papadopoulos, Endpoint-Side Optimization of a Five Degree-of-Freedom Haptic Mechanism, *Proc. IEEE 13th Mediterranean Conference on Control and Automation*, Limassol, Cyprus, 2005.

[16] E. Papadopoulos, A. Tsamis, & K. Vlachos, A Real-Time Graphic Environment for a Urological Operation Training Simulator, *Proc. IEEE Int. Conference on Robotics and Automation*, New Orleans, Louisiana, 2004, 1295-1300.